# *Impurity transport, turbulence transitions and intrinsic rotation in Alcator C-Mod plasmas*

PSFC/JA-13-62

# Impurity Transport, Turbulence Transitions, and Intrinsic Rotation in Alcator C-Mod Plasmas

N.T. Howard[1], A.E. White[2], M. Greenwald[2],
C. Holland[3], J.Candy[4], and J.E. Rice[2]

[1]Oak Ridge Institute for Science and Education (ORISE), Oak Ridge, TN 37831, USA
[2]MIT Plasma Science and Fusion Center, Cambridge MA 02139, USA
[3]University of California - San Diego, La Jolla, CA 92093, USA
[4]General Atomics, San Diego, CA 92121, USA

December 2013

**Plasma Science and Fusion Center**
**Massachusetts Institute of Technology**
**Cambridge MA 02139 USA**

This work was supported by the U.S. Department of Energy, Grant No. DE-FC02-99ER54512-CMOD and DE-SC0006419. 

# Impurity Transport, Turbulence Transitions, and Intrinsic Rotation in Alcator C-Mod Plasmas

**N.T. Howard[1], A.E. White[2], M. Greenwald[2], C. Holland[3], J. Candy[4], and J.E. Rice[2]**

[1] Oak Ridge Institute for Science and Education (ORISE), Oak Ridge, TN 37831, USA

[2] MIT Plasma Science and Fusion Center, Cambridge MA 02139, USA

[3] University of California - San Diego, La Jolla, CA 92093, USA

[4] General Atomics, San Diego, CA 92121, USA

**Abstract.** Linear and nonlinear gyrokinetic simulations are used to probe turbulent impurity transport in intrinsically rotating tokamak plasmas. For this simulation-based study, experimental input parameters are taken from pair of ICRF heated Alcator C-Mod discharges exhibiting a change in the sign of the normalized toroidal rotation gradient at mid radius (i.e. a change from hollow to peaked intrinsic rotation profiles). The simulations show that there is no change in the peaking of the calcium impurity between the plasmas with peaked and hollow rotation profiles, suggesting that the impurity transport and the shape of the rotation do not always change together. Furthermore, near midradius, r/a =0.5 (normalized midplane minor radius), the linear and nonlinear gyrokinetic simulations exhibit no evidence of a transition in linear dominance from Ion Temperature Gradient (ITG) to Trapped Electron Mode (TEM) when the intrinsic rotation profile changes from peaked to hollow. Extensive nonlinear sensitivity analysis is performed, and there is no change in the ITG critical gradient or in the stiffness of ion heat transport with the change in the intrinsic toroidal rotation profile shape, which suggests that the shape of the rotation profile is not dominated by the ITG onset in these cases.

## 1. Introduction

Understanding and controlling the core confinement of impurities is of great interest in the fusion community. Accumulation of impurities in the core of ITER plasmas could lead to excessive radiation of power and dilution of the fuel, ultimately resulting in deleterious effects on the overall energy balance. Understanding the mechanisms responsible for accumulation and expulsion of impurities from the plasma core is vital for the success of any fusion reactor. In current day machines, large co and counter injected neutral beams are often used to tailor the toroidal velocity profile in the plasma core, leading to significant local E×B shearing rates, an overall reduction in the core turbulence, ultimately enhancing core energy confinement. However, the large size and high density of ITER plasmas is expected to limit the penetration of neutral beams into

the core, placing limits on the use of neutral beams to achieve some high performance scenarios. It is therefore important to study transport of impurities under reactor relevant plasma conditions in situations with little to no external momentum input; i.e. when the toroidal rotation profile is intrinsically generated. While the causes of intrinsic rotation in tokamaks are not well understood, both experimental observations and leading theories suggest that momentum transport is primarily driven by turbulence [1]. In particular, quasilinear theory shows that near ITG marginality, momentum transport is dominated by an inward turbulent equipartition momentum pinch [2, 3], a subset of the more general Coriolis pinch [4, 5].

In addition to the important role turbulence likely plays in determining the intrinsic rotation profile in tokamaks, turbulence can play an important role in setting experimental levels of impurity transport[6, 7, 8, 9, 10]. Therefore, predicting the transport of impurities in ITER may be linked to prediction of the intrinsic toroidal rotation in ITER, since the local E×B shearing rates will affect the turbulence and modify the impurity transport. Beyond the effects of ExB shearing rates, it has been suggested that the rotation may also affect the background turbulence in a different manner. This interpretation arises from JET experiments demonstrating a correlation between plasmas with higher values of toroidal rotation and stiffness of the ion temperature profile. [11, 12]. However, recent gyrokinetic work suggests that the observed correlation may not result from a direct relationship between the stiffness and rotation but instead may be explained by electromagnetic effects and the presence of significant fast ion populations in the discharges studied [13, 14].

In recent years, theoretical [1, 2, 3, 6, 15, 16, 17, 18, 19] and experimental [20, 21, 22, 23, 24, 25] work throughout the fusion community has focused on understanding turbulent impurity and momentum transport and their connections in the tokamak core. Several experiments have noted that changes in the toroidal rotation profile shape, from peaked to hollow, are possibly related to the transition from linear ITG to TEM dominance. These observations have been made in LOC/SOC plasmas [21, 24], and in plasmas with auxiliary wave heating [26, 22]. Theoretically, changes in the direction of the residual stress contribution to the momentum transport can change sign for ITG versus TEM turbulence [15]. However, there is open debate regarding this issue[18, 20]. Linear gyrokinetic simulations have shown that the normalized toroidal rotation gradient at midradius changes sign across the linear ITG to TEM dominance transition, consistent with observations at ASDEX-U [18]. It has also been shown at ASDEX-U experimentally that when ECRH power is added to NBI heated H-modes, the impurity ion density profiles will peak and the core toroidal rotation will flatten [22]. In these plasmas, linear gyrokinetic simulations showed that the dominant turbulence regime transitioned from ITG to TEM (the ECRH modifies the electron and ion temperature profiles so as to favor the TEM). The peaking of the impurity density is attributed to the change from linear ITG to TEM dominance, and importantly, across the ITG to TEM transition, there were clear changes in both the momentum and impurity particle transport.

In this paper, we perform linear and nonlinear gyrokinetic analysis using the GYRO code [27] to explore the relationships between the peaking of impurity profiles, the shape (hollow vs. peaked) of intrinsic toroidal rotation profiles, and changes in the ITG/TEM instability. The input parameters for these simulations are based on experimental data from a pair of Alcator C-Mod discharges [28, 29]. These discharges were operated with almost identical engineering parameters, yet display a toroidal rotation reversal and therefore exhibit peaked and hollow toroidal rotation profiles (Figure 1), making them an ideal testing ground for this study. For the remainder of this paper we will refer to the discharges with peaked and hollow toroidal rotation as the peaked and hollow discharges.

Experimental and simulation results from the peaked and hollow discharges have been reported recently [29]. For this paper, the analysis has been updated to include improved toroidal rotation and an analysis window that spans from 1.0 to 1.4 seconds. This updated analysis utilizes line-integrated toroidal rotation measurement provided by Alcator's X-ray Imaging Spectrometer (XICS) [30, 31] and b-spline fitting of the measurement to provide more reliable profiles of toroidal rotation and quantities reliant on its derivative (such as E $\times$ B shear). Section II will cover a brief description of the experimental measurements and simulation setup. Section III of this paper covers a quantitative comparison of new global simulations with experimental impurity transport coefficients in an attempt to resolve a previous discrepancy between simulation and experiment. Section IV focuses on a scan of the ITG drive term, $a/L_{T_i}$ performed using nonlinear gyrokinetic simulation. This section examines possible links between toroidal rotation, the ITG critical gradient, and stiffness of the ion heat transport. Section V describes an extensive nonlinear gyrokinetic simulation sensitivity scan of TEM drive terms that is designed to search for signs of an ITG to TEM transition in the peaked and hollow discharges. Finally, Section VI will include a brief description of the results and discussion.

## 2. Description of the Experimental and Gyrokinetic Simulation Setup

### *2.1. Experimental Setup and Analysis*

In this paper we discuss simulation results based on two Alcator C-Mod L-mode discharges. Alcator C-Mod is a compact (R= 0.68m, a = 0.22 m), high density ($n_e(0)$ up to $1 \times 10^{21}$ m$^{-3}$), high field ($B_T$ up to 8.0 T), tokamak located at the MIT Plasma Science Fusion Center in Cambridge, MA. It has significant plasma shaping and auxiliary heating capabilities via Ion Cyclotron Resonance Heating (ICRH) ( $P_{ICRH} \leq 6.0$ MW). The two plasmas studied in this paper are operated with effectively identical plasma conditions including fixed plasma shape ($\kappa = 1.6$), current ($I_p = 0.8$ MA), ICRH input power ($P_{ICRH}$=1.2 MW), and magnetic field ($B_T$=5.4 T). These two discharges only differed in their respective density profiles (obtained via edge gas puffing), with core densities of approximately 1.4 and $1.55 \times 10^{20}$ m$^{-3}$ (See Figure

2). However, this slight increase in density resulted a reversal of the toroidal rotation direction on axis and rotation profiles that transitioned from peaked to hollow (Figure 1). Throughout the paper we will reference the Mach number and rotation gradient of these plasmas, using the definition used in References [18, 16] for comparison. We define the Mach number for species x, as $u = v_\phi/v_{th,x}$ and the toroidal rotation gradient as $u' = -(R^2/v_{th,x})d\omega/dr$ where $\omega$ is the toroidal angular rotation frequency and $v_{th,x} = \sqrt{2T_x/m_x}$ is the thermal velocity for species x. For the peaked (hollow) discharges we find values of $u \sim 0.09(0.02); u' = 0.55(-0.30)$ for the main ions and $u \sim 0.39(0.1); u' = 2.5(-1.4)$ for the calcium impurities studied. All analysis presented in this paper will focus on stationary portions of the discharges from 1.0 to 1.4 seconds, a period that is substantially longer than the energy confinement time ($\sim$ 30 ms). Both of these discharges were operated in upper single null with the ion $\nabla B$ drift away from the active X-point. This operational choice raises the H-mode power threshold, allowing the plasma to maintain an L-mode state at higher input powers. Almost all discharges operated on Alcator C-Mod have the presence of an internal q=1 surface and therefore demonstrate sawtooth activity. Sawteeth were present in both discharges throughout the entirety of the analysis window. We therefore have restricted all simulation work to occur outside of the sawtooth inversion radius ($\sim$ r/a = 0.38 to 0.40) to minimize the impact of this phenomenon.

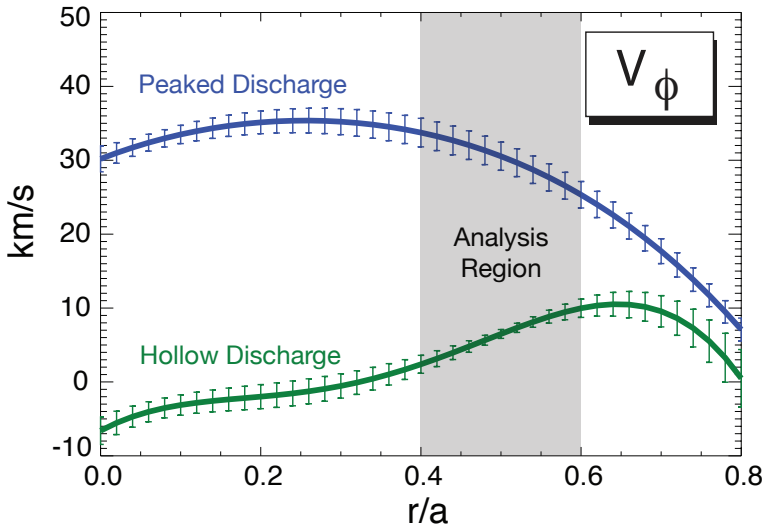


**Figure 1.** (Color Online) Time averaged (1.0 to 1.4 sec), fits to the toroidal rotation profiles obtained from the Xray Imaging Crystal Spectrometer (XICS) are plotted for the peaked (blue) and hollow (green) discharges. All analysis focuses on the region r/a = 0.4 to 0.6

As this paper is primarily dedicated to new simulation results, the reader is directed to a series of published work for a description of the experimental measurements. The suite of diagnostics used for the experimental analysis is identical to previous work and can be found in references [29], [32], and [28]. The experimental impurity transport

described in this paper has been reported in reference [29] and an in-depth review of the analysis technique can be found in reference [10].

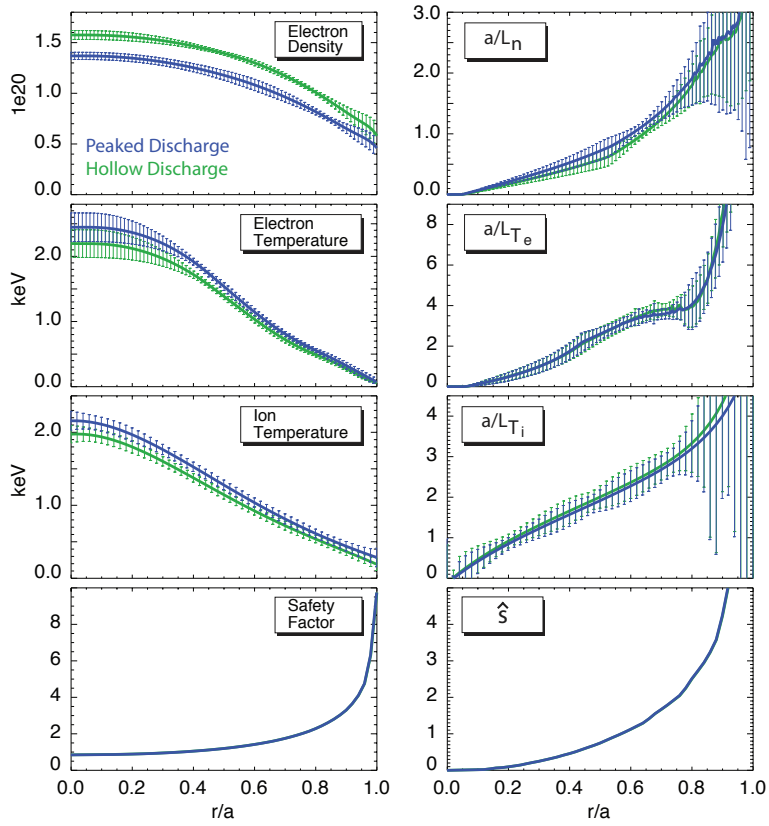


**Figure 2.** (Color Online) Time averaged (1.0 to 1.4 sec) plasma profiles and their corresponding turbulence drive and suppression terms are plotted for the peaked (blue) and hollow (green) discharges.

Estimated uncertainties on the turbulence drive terms, $a/L_{T_e}$, and $a/L_n$ were determined from the standard deviation of each profile during the analysis period. Uncertainties on the ion temperature profiles attempted to include the effects of known systematics as well as fitting errors (see Figure 2). In the region of interest, r/a =0.4 to 0.6, we have estimated the uncertainties in these quantities to be $\pm 15 - 20\%$ in $a/L_{T_i}$ and $\pm 10 - 15\%$ in $a/L_{T_e}$, and $a/L_n$. These uncertainties will be used in the following sections to provide a basis for the sensitivity analysis performed and we note that all uncertainties quoted in this paper are $1\sigma$ uncertainties. The heat fluxes reported throughout this paper as the "experimental" heat fluxes are results of the power balance TRANSP [33]. TRANSP takes measured plasma profiles as inputs and uses internal RF deposition models to calculate the experimental heat fluxes. A more in-depth description of the estimates in the profiles and experimental heat fluxes can be found in [10] and [32].

### *2.2. Linear and Nonlinear Simulation Setup*

The simulation work presented in this paper utilized the GYRO code [27]. Both local (r/a = 0.5) and global nonlinear simulations are presented here to make quantitative comparisons with experimental heat fluxes and impurity transport coefficients. All simulations were electrostatic, used Miller geometry [34], and a 128 point velocity space discretization (8 pitch angles, 8 energies, and 2 signs of velocity), which has been demonstrated previously to provide accurate simulation results [35]. Each local simulation included 3 kinetic species: deuterium ions, electrons, and the dominant impurity species in Alcator C-Mod (boron) while the global simulations, to determine the simulated impurity transport, included an additional 2 trace species of calcium. Rotation effects (E×B rotation shear, Coriolis drift effects, and parallel flow gradients) were included in each simulation with the electrons treated drift-kinetically and both ion-ion and electron-ion collisions included. Details of the collision model and other aspects of GYRO can be found in Reference [36]. To adequately capture the dynamics of the ion-scale turbulence, both the local (global) nonlinear simulations utilized 24 (20) toroidal modes and extended up to approximately $k_\theta \rho_s = 1.25 \leftrightarrow 1.4$. Here, $\rho_s = c_s/\Omega_{ci}$ is the sound speed gyroradius, $\Omega_{ci} = eB/m_i c$ is the ion frequency, $c_s = \sqrt{T_e/m_i}$ is the sound speed evaluated at the center of the simulation domain (r/a = 0.5), $B = 1/r\ d\chi_t/dr$ is the effective magnetic field, and $\chi_t$ is the toroidal flux divided by $2\pi$. The normalized gradient scale length, $a/L_x$ (for arbitrary parameter x), which will be referred to throughout the text, are given by $-a\nabla x/x$. These numerical settings resulted in physical simulation box sizes in the radial and binormal directions of approximately $100 \times 100\rho_s$ for the local simulations and approximately $90 \times 90\rho_s$ in the global simulations. The global runs presented here spanned from approximately r/a = 0.35 to r/a = 0.65. However, the comparisons presented in the next section will focus on the region r/a = 0.4 to 0.6, where the impurity transport measurements and simulation results are most reliable. All local simulations utilized 350 radial grid points for a grid spacing of $0.33\rho_s$ while global runs utilized only 320 radial grid points for the same approximate radial grid spacing. All quantities obtained from the gyrokinetic simulations were time averaged over long simulation times ($\sim$ 400 a/c$_s$ or longer ) to ensure reliable results.

The impurity transport coefficients extracted from global simulations were obtained in manner reported previously [10]. Two trace species of He-like calcium (Z = 18) were inserted into each simulation at a concentration of $n_z/n_e = 0.0001$ and we note that they are assumed to have constant impurity density on a flux surface. These species only differed in their density gradients which were specified to be $\pm$50% changes from the electron density gradient. Plotting the simulation output values of $\Gamma/n_z$ versus $\nabla n_z/n_z$ allows for determination of the diffusion coefficient and convective velocity from the slope and y-intercept of the fitted line. We note that the impurity particle flux spectra in these simulations tend to peak at relatively low values of $k_\theta \rho_s$ ($\sim$ 0.4) for both plasmas studied and the contributions to the impurity fluxes have dropped to less than 1/10th

of their peak value by the highest simulated wavenumber, suggesting resolving smaller scales would result in negligible contributions to the impurity fluxes.

The approach used to perform the nonlinear simulations is briefly summarized here for completeness but can be found in more detail in references [10, 37, 29, 32]. The gyrokinetic simulations performed for this work focus only on long wavelength contributions to the heat flux ($k_\theta \rho_s \leq 1.0$ ) and neglect contributions from electron-scale turbulence. The inclusion of electron-scale turbulence may play a significant role in setting the overall electron heat flux, but has previously been observed to provide relatively little increase in the ion heat flux [38, 39, 40]. Therefore, small modifications to the experimental turbulence drive terms, always within experimental uncertainty, were made to match the simulated ion heat flux with the experimental value while agreement in the electron channel was ignored. As demonstrated in Sections IV and V, both discharges investigated are ITG dominated at the location of interest (r/a = 0.5). With this observation, modifications were made to the ITG drive term, $a/L_{T_i}$ to match the simulated and experimental heat fluxes. All of the global simulations reported here as well as the local nonlinear simulation base cases (at r/a = 0.5) are ion heat flux-matched simulations. We note that no discussion of the simulated momentum fluxes will be presented here. Due to a lack of symmetry breaking mechanisms, comparisons between GYRO simulation and experimental momentum fluxes in intrinsically rotating plasmas is not possible at this time. For more details, see reference [29] and references therein.

## 3. Quantitative Comparison of Measured Impurity Transport with Nonlinear Simulation

Earlier work reported by White *et al.* made quantitative comparisons of gyrokinetic simulation with experimental impurity transport in both the peaked and hollow discharges [29]. The peaked discharge displayed quantitative agreement between simulation and experimental impurity transport across most of the profile studied while a disagreement between the simulated and experimental impurity diffusion coefficient was found across the simulated domain (r/a = 0.4 - 0.6) in the hollow discharge. Although simulations were never performed to demonstrate agreement, it was speculated that small adjustments to the dominant turbulence drive, $a/L_{T_i}$, could resolve this discrepancy. In this section we present an attempt to use the updated analysis (time averaged input profiles and fitted rotation profiles) to perform new global simulations that resolve the previous discrepancy between simulation and experiment in the hollow discharge and improve upon the previous simulation of the peaked discharge. Additionally, we discuss the observed changes in the simulated impurity transport and its relationship to the measured changes in the toroidal rotation profiles.

The results from an ion heat flux-matched global simulation of the peaked discharge are presented in Figure 3 where the impurity transport diffusion and convection coefficients, D and V, are plotted in panels a and b with the ion and electron heat fluxes

plotted in panels c and d. It may be noted that the final, ion-heat flux-matched profiles of $a/L_{T_i}$ used in both the peaked and hollow simulations varied from the previous work by typically $< 10\%$ across the simulation domain when compared to the previous work [29]. For comparison with the turbulence driven impurity transport, the neoclassical impurity transport coefficients from both discharges are plotted in Figures 3 and 4. Local simulations were performed using the neoclassical transport code NEO [41]. These simulations used Miller geometry, toroidal rotation effects, and 5 species (deuterium, electrons, boron, and 2 trace calcium species). As shown in Figures 3 and 4, they demonstrate a negligible role of neoclassical transport in the region of interest for these discharges.

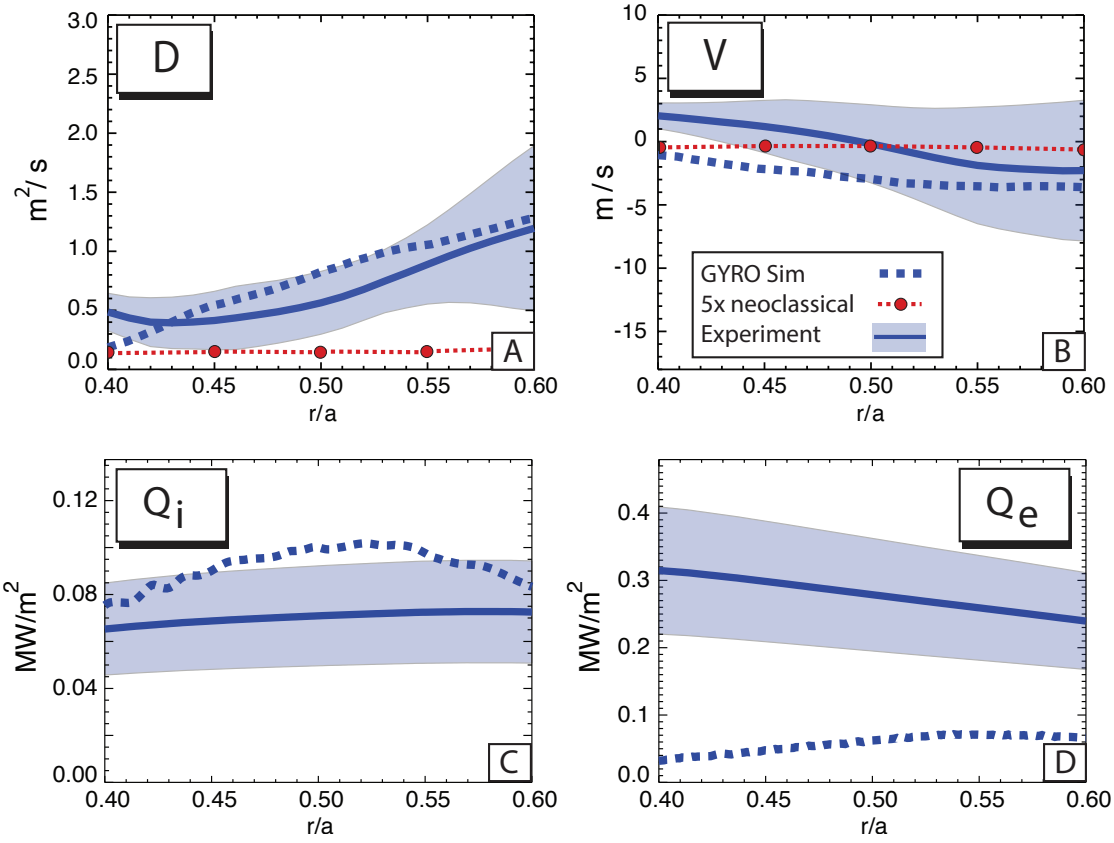


**Figure 3.** (Color Online) The results from an ion-heat flux matched global gyrokinetic simulation are shown for the peaked discharge. Comparisons are made with measured levels of impurity transport (panels a and b) as well as heat fluxes (c and d). Agreement is generally found with measured ion heat flux and impurity transport coefficients

This simulation displays approximate agreement with the upper error bar of the experimental ion heat flux while under predicting the electron heat flux across the entirety of the simulated profile (r/a = 0.4 to 0.6). This discrepancy in the electron heat flux channel has been observed in a large number of Alcator C-Mod discharges [10, 37, 32]. It is believed that it arises from the electron-scale turbulence that is excluded from standard ion-scale gyrokinetic simulation. This is the subject of ongoing model

validation work but is out of the scope of this paper. Despite missing contributions to the electron heat flux, this new global simulation finds agreement within the diagnosed uncertainties between the simulated and experimental values of the impurity diffusion coefficients across a majority of the simulation domain. Similar agreement is found in the convective velocity outside of approximately r/a =0.48 with some slight disagreements found inside of this radial location. The results from the peaked discharges analysis are found to be in general quantitative agreement with that reported previously [29].

In an attempt to resolve the previous disagreement in the diffusion coefficient, identical analysis was performed on the hollow discharge. The results of this analysis are plotted in Figure 4. The simulated ion heat flux obtained from the previous analysis approximately matched the mean experimental heat flux. In contrast, the new ion heat flux-matched simulations have slightly different ion temperature profiles and match the simulated ion heat flux at the upper error bar of the experimental value.

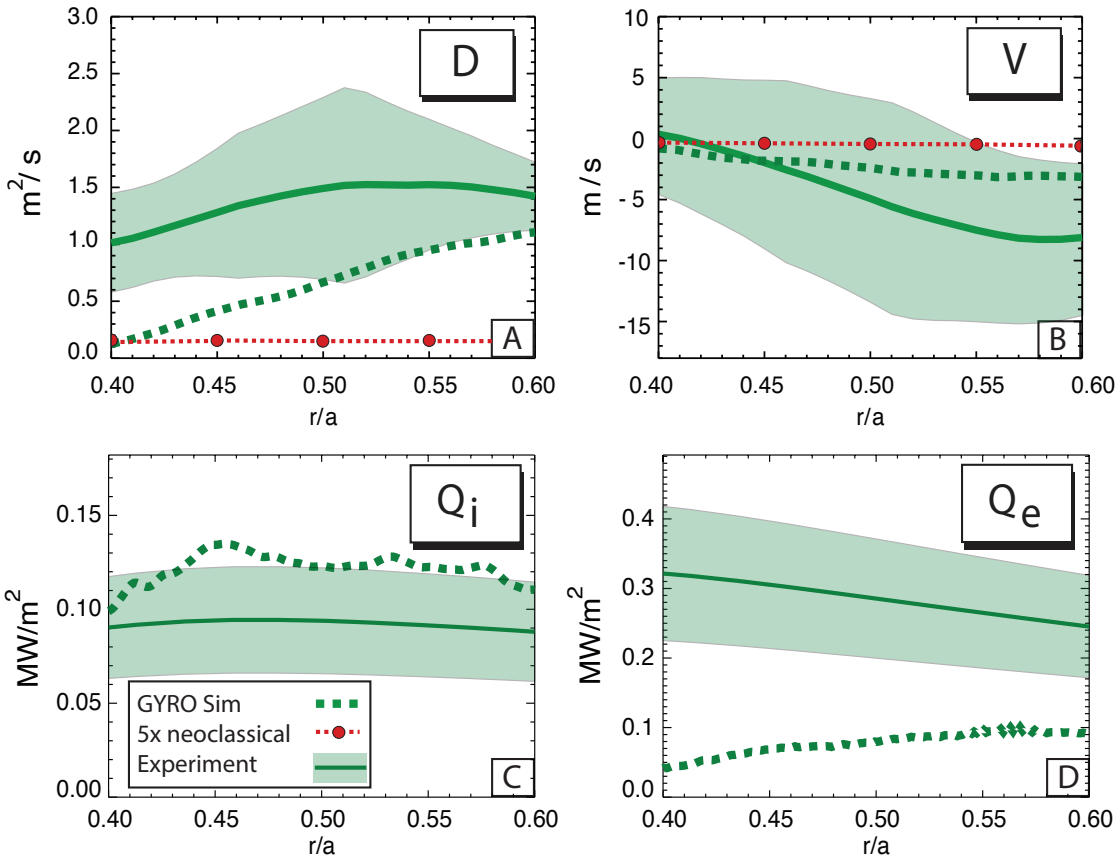


**Figure 4.** (Color Online) The results from an ion-heat flux matched global gyrokinetic simulation are shown for the hollow discharge. Comparison are made with measured levels of impurity transport (panels a and b) as well as heat fluxes (c and d). Decent agreement is generally found with measured ion heat flux and impurity transport coefficients, although some discrepancy with the diffusion coefficient still remains

This small adjustment to the ion temperature tends to enhance the overall level of the impurity transport and therefore results in a slightly higher simulated diffusion

coefficient and larger inward convective velocity. We note that this ion heat flux-matched simulation exhibits a similar under-prediction of the electron heat flux to that found in the peaked discharge. Given the similarity in the input parameters and linear stability analysis (see Figure 6), this result is unsurprising. Compared with previous results, it appears as though the simulated diffusion coefficient has improved agreement with the experiment. Although some discrepancy between simulation and experiment remains, the simulated diffusion coefficient is found to be in agreement with experiment outside of r/a = 0.5 with the convective velocity displaying agreement across the simulation domain. It is important to note that for both discharges, the location of the sawtooth inversion radius is approximately r/a = 0.38 to 0.4. Although relatively small, disagreement at inner radii (Figures 3b and 4a) may be related to the influence of sawtooth activity, neoclassical contributions, sensitivity to a driving gradient not explored in this work, or some combination of these mechanisms.

The analysis technique used to extract the experimental values of D and V from measured calcium emission attempts to assess uncertainty in these values resulting from error in the background plasma profiles. Unfortunately, for the studied discharges, the resulting uncertainties on the experimental impurity peaking do not allow for any statement of changes in impurity peaking to be made. Any change in the impurity peaking is obscured by the error bars obtained for this dataset. An initial analysis of argon emissivity profiles for the peaked and hollow discharges does suggest a larger peaking of impurities in the core of the hollow discharge. However, a full analysis of this data has not been performed and is left for future experimental impurity transport analysis.

Despite limitations in the impurity transport data, comparison can be made between the peaked and hollow impurity peaking obtained from the simulation results. Observations from ASDEX-Upgrade suggest a strong link between changes in toroidal rotation, rotation gradient, and boron impurity transport [22, 16]. However, as seen in Figures 3b and 4b the direction of the simulated impurity convection is inward (negative) for both discharges. This result holds for all simulations performed while trying to obtain ion heat flux-matched simulation and appears robust for simulation results constrained to match the experimental ion heat flux. The presence of inward impurity convection implies peaked profiles of the calcium impurities in both discharges, suggesting no strong link between the observed rotation changes and impurity peaking.

However, it is important to note that the ASDEX-Upgrade results span a wide range of Mach numbers (u) and rotation gradients (u'). The main ion and calcium Mach numbers and rotation gradients, evaluated in a manner consistent with the ASDEX results are given in Section 1 of this text. We determine that although the Mach number range is more limited than the ASDEX-Upgrade results, the range of rotation gradient spanned by the peaked and hollow discharge is equivalent to approximately half of the range covered in references [22, 16]. Casson, *et al.* report a strong scaling of measured boron transport with rotation gradient. However, we note that the C-Mod discharges studied here display weak or little response of the impurity transport

to the differences in rotation gradient. Overall, we conclude that nonlinear gyrokinetic simulation demonstrates quantitative agreement with experimental ion heat flux and impurity transport over most of the range studied and that the simulated impurity peaking does not appear to track the observed transition in toroidal rotation for these discharges.

## 4. Toroidal Rotation, the ITG Critical Gradient, and Ion Stiffness

In 2009, results from the JET tokamak were reported by Mantica *et al.* that indicated a link between measured toroidal rotation and ion stiffness [11]. With increased values of toroidal velocity, a decrease in the ion stiffness was observed. However, very recent work utilizing the GENE code [42] and reported by Citrin *et al.* indicates that the reduction of ion stiffness with toroidal rotation on JET may be explained by stabilization of ITG by electromagnetic effects and fast ions [13, 14]. Despite the fact that the two discharges reported here are at significantly smaller Mach numbers than the JET results, their angular rotation frequencies are comparable to this previous work and they provide another test of the role of toroidal rotation on stiffness and the ITG critical gradient. The peaked and hollow discharges are extremely similar in engineering parameters (only varying in the density) and demonstrate significantly different values of the toroidal rotation at mid-radius (r/a = 0.5), where the profiles of ion and electron temperature, rotation, and electron density are well diagnosed. Although opposite in sign, the local value of the $E \times B$ shearing rate at the analysis location is similar ( abs($\gamma_{ExB}$) (in a/$c_s$) = 0.023 (0.018) for peaked (hollow) ) between the two discharges and 3-4× smaller than the peak of the low-k linear growth rate (Figure 6) . This eliminates some uncertainty in the results imposed by differences in E × B shear which is known to have significant effects on the ITG critical gradient and low-k turbulence dynamics.

Analysis was performed at mid-radius to exploit the significant difference in the local values of rotation. The local values of XICS measured toroidal rotation are $\sim$ 7 km/s for the hollow discharge and 30 km/s for the peaked discharge at r/a=0.5. Local, nonlinear gyrokinetic simulation was performed at this location with almost identical simulation parameters to those described in Section II. We note that these simulations neglected ion-ion collisions but were otherwise numerically identical to the local simulations presented in the following section. This difference in the simulation setup was found to have no significant effect on the conclusions presented in this section but is mentioned for completeness. To probe both the ITG critical gradient and the stiffness at these locations, the value of the ITG drive term, $a/L_{T_i}$ was varied from its experimental value down to 70% of its experimental value using 14 separate simulations. This scan more than sufficiently reveals the location of the ITG critical gradient and allows us to understand the response of the ion heat flux to changes in the turbulence drive. In Figure 5 the ion heat flux obtained via nonlinear simulation is plotted versus the ITG drive term.

We find that despite a significant difference in the local value of toroidal rotation,

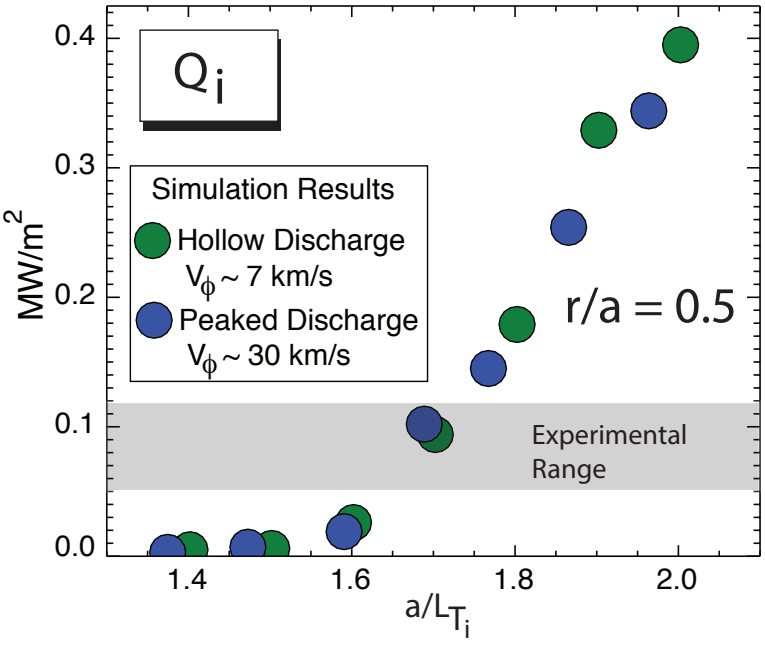


**Figure 5.** (Color Online) Nonlinear gyrokinetic simulation at r/a = 0.5 is presented for the peaked and hollow rotation discharges. The simulated heat fluxes from the peaked (blue) and hollow(green) discharges are shown for a scan of the ITG drive term, $a/L_{T_i}$. The x intercept of this plot is indicative of the ITG critical gradient and the slope is indicative of the ion stiffness in these plasmas.

there is no recognizable difference in the value of the ITG critical gradient in these discharges, denoted approximately by the x intercept of the ion heat fluxes. Both discharges appear to have simulated heat fluxes that approach zero at a value of the ITG drive term, $a/L_{T_i}$ equal to approximately 1.57. The location of the experimental ion heat fluxes relative to the nonlinear critical gradient is also effectively identical in these plasmas. Both discharges sit less than 10% above the nonlinear threshold, suggesting the plasma conditions are marginally stable to ITG. This result is interesting in the context of the observed changes in the toroidal rotation. Work by Hahm [2] and Yoon [3] suggests that near marginally ITG stability, the inward turbulent equipartition momentum pinch plays a dominant role and is directed inward for typical plasma parameters. Despite both of the studied plasmas exhibiting marginally stability to ITG turbulence, they display a robust reversal of their toroidal rotation profiles, suggesting the physics of the peak to hollow transition is not dominated by the mechanism proposed by Hahm and Yoon for these discharges.

Examining the slope of ion heat flux plotted versus the ITG drive term for values above the ITG critical gradient provides information on the local ion stiffness predicted by the simulation. Both discharges appear to respond extremely strongly to changes in the ITG drive, with a $15-20\%$ increase in this drive resulting in up to a 450% increase in the driven heat flux. These ion-scale simulations suggest that the dependence of the ion heat flux on $a/L_{T_i}$ is identical between the peaked and hollow discharges, implying

identical ion stiffness at substantially different values of toroidal rotation. Although no data from dedicated experimental scans of the ion heat flux was collected for comparison, we note that the ion temperature profile shapes obtained from the peaked and hollow discharges are nearly identical, consistent with similar levels of ion stiffness in the plasma core and the results of this nonlinear gyrokinetic analysis. On Alcator C-Mod we therefore find no significant effect of toroidal rotation on ion stiffness, consistent with the results from Citrin *et al.* [13, 14].

## 5. Search for ITG/TEM Transition Using Nonlinear Gyrokinetic Simulation

Links between impurity transport, ITG/TEM stability, and toroidal rotation have been explored both experimentally [22, 16], and theoretically [6, 18]. It has been proposed that the transition from Linear to Saturated Ohmic Confinement regimes (LOC to SOC) and the accompanied reversal of the toroidal rotation [23, 43] are the result of a transition from TEM to ITG dominated plasma turbulence[24, 18, 44, 45]. Reversal or hollowing of the toroidal rotation profile in auxiliary heated plasmas has been observed more recently [26, 28] and has been attributed to the same underlying transition of the turbulence [22]. To date, these conclusions have been based predominantly on low-k ($k_\theta \rho_s < 1.0$) linear stability analysis performed in the plasma core. In this paper we perform nonlinear gyrokinetic analysis at the mid radius to search for evidence of an ITG to TEM transition in the peaked and hollow discharges. This location is just inside of the radial location where the rotation profiles deviate significantly (see Figure 1) and might be expected to exhibit signatures of ITG/TEM transition.

To understand the low-k ($k_\theta \rho_s < 1.0$) linear stability, initial value, linear gyrokinetic analysis was performed on both the peaked and hollow discharges at r/a = 0.5. The results of this analysis are detailed in Figure 6 for the peaked (panels a and b) and hollow discharges (panels c and d) respectively. The real frequencies and growth rates from analysis using all experimental inputs are plotted together with the values obtained from the ion heat flux-matched conditions. As these plasmas have similar values of the turbulence-relevant parameters ( $a/L_{T_i}$, $a/L_{T_e}$, $a/L_n$, and $\hat{s}$), it is not surprising the linear stability from these discharges exhibit very similar characteristics. For parts of the linear spectrum below $k_\theta \rho_s \sim 0.95$, the most unstable linear modes rotate in the ion diamagnetic drift direction (negative by GYRO conventions) and respond sensitively to changes in the ITG drive, above this value of $k_\theta \rho_s$ the TEM/ETG branch appears to dominate the spectrum with unstable modes rotating in the electron direction (positive real frequency). It is expected that a majority of transport is driven by the longer wavelengths associated with the lower values of $k_\theta \rho_s$. For this reason, we classify both the discharges are being ITG dominated with perhaps some subdominant TEM contributions. However, to understand how the turbulent state of these plasmas and to investigate any effects of subdominant modes, we turn to nonlinear simulation of these discharges at r/a = 0.5.

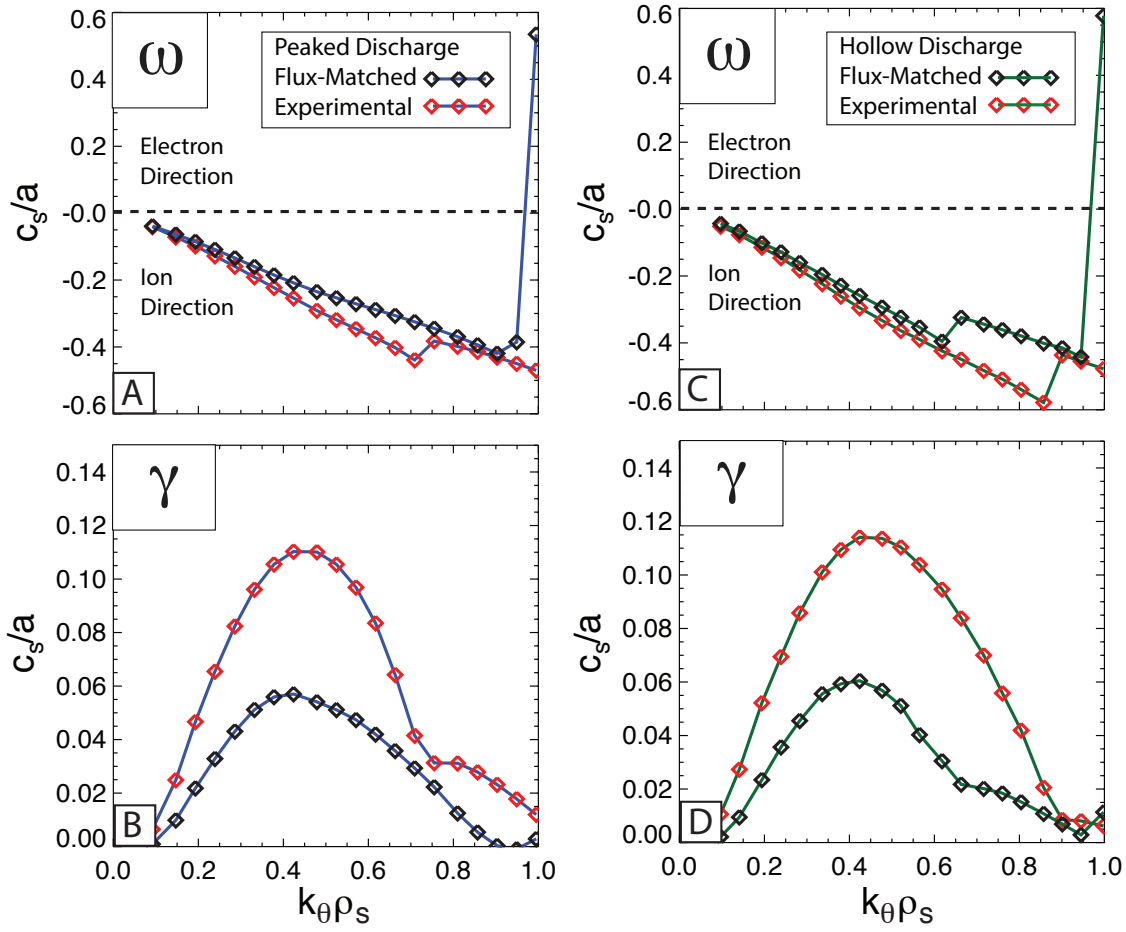


**Figure 6.** (Color Online) Results from low-k linear gyrokinetic simulation are plotted for the peaked (a & b) and hollow (c & d) discharges for the experimental gradients (black diamonds) and those used in the ion heat flux-matched simulation (red diamonds).

Local, nonlinear sensitivity scans were used to search for evidence of an ITG to TEM transition in the peaked and hollow discharges. All of the simulations presented in this section were based around the ion heat flux-matched, base case simulations for both discharges. As the response of the simulation results to changes in the ITG drive term was studied in the previous section, we focused this sensitivity analysis on scans of known TEM drive terms to search for evidence of an ITG/TEM transition. These variations included scans of $a/L_{T_e}$, $a/L_n$, and $\nu_{ei}$ within estimated $1\sigma$ uncertainties ($\pm 15\%$ in $a/L_{T_e}$, $\pm 15\%$ in $a/L_n$, and $\pm 20\%$ in $\nu_{ei}$). This analysis resulted in 12 total simulations performed at r/a = 0.5 in the hollow and peaked discharges. The resulting ion and electron heat fluxes obtained from these scans can be found in Figures 7 and 8.

In contrast to the extreme sensitivity to the ITG drive term, $a/L_{T_i}$ found in Section IV (Figure 5), the peaked discharge displays only weak dependencies to all of the TEM drives. Both the ion and electron heat fluxes appear to slightly decrease with increased collisionality and slightly increase with increased values of $a/L_n$. However, we note that

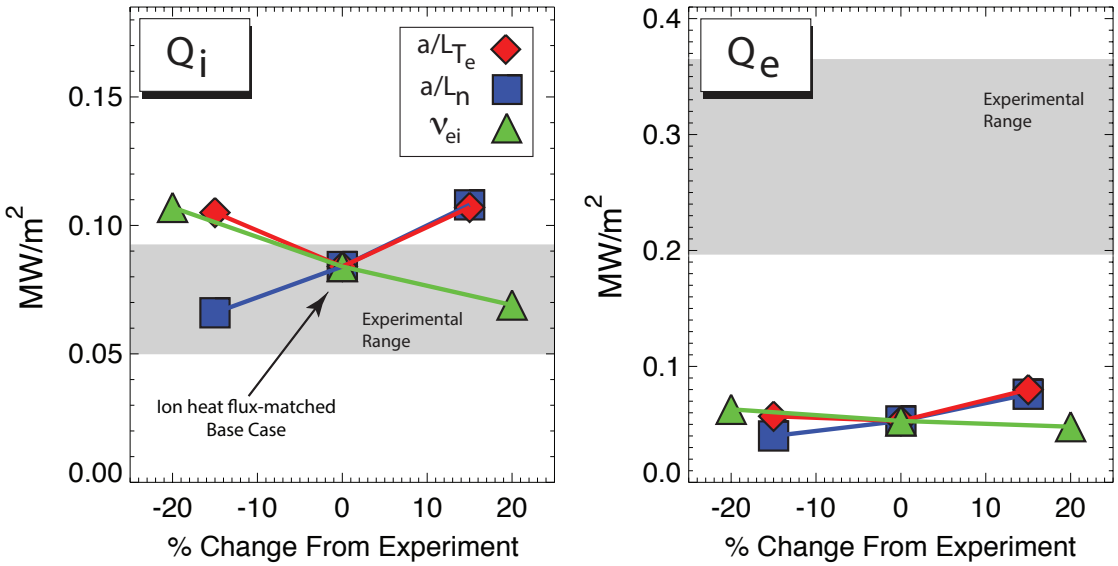


**Figure 7.** (Color Online) Response of the nonlinear heat fluxes to changes in TEM drive terms are shown. The response of these quantities to $1\sigma$ increases/decreases in $a/L_{T_e}$ (red), $a/L_n$ (blue), and $\nu_{ei}$ (green) around the ion heat flux-matched base case are plotted for the peaked discharge

a $1\sigma$ change in these parameters results in only an approximately 25% modification of simulated heat flux. To remind the reader, Figure 5, indicates that a $1\sigma$ increase in $a/L_{T_i}$ results in an approximately 450% change in the simulated heat flux. Therefore no strong evidence for an ITG to TEM transition is found when examining purely the sensitivity of the simulated heat fluxes to changes in the TEM drive terms for the peaked discharge. Furthermore, none of the variations reported here come even remotely close to simultaneous matching of the ion and electron heat fluxes. As discussed earlier, this observation is believed to be the result of missing high-k, electron-scale turbulence in these simulations. Resolution of this discrepancy is out of the scope of this work but is the subject of ongoing investigation.

The identical analysis was performed on the hollow discharge and is reported in Figure 8. The results from the nonlinear scans are nearly identical to those found in analysis of the peaked discharge with a slightly increased sensitivity to changes in electron-ion collisionality and a slightly reduced sensitivity to changes in $a/L_n$. The observed trend with collisonality can be explained by a decrease in the Dimits shift and the value of the ITG critical gradient at decreased electron-ion collisionality. It was shown by Mikkelsen *et al.* that decreases in collisionality result in a downward shift of the ITG critical gradient [46]. Therefore, at a constant value of $a/L_{T_i}$ one observes an increase in the overall ion and electron heat fluxes due to increased strength of the ITG, and not an overall increase in TEM activity. Neither discharge is observed to have a meaningful trend with $a/L_{T_e}$ suggesting a minimal presence of electron temperature gradient driven TEMs. We conclude that this analysis does not identify any signatures of an ITG/TEM transition in either the peaked or the hollow discharges at r/a=0.5.

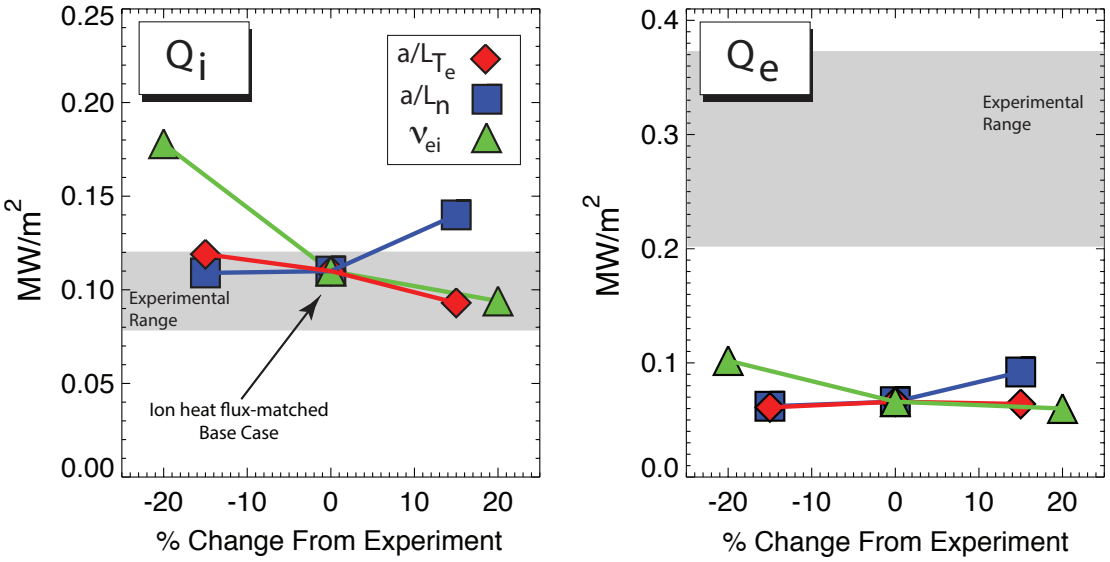


**Figure 8.** (Color Online) Response of the nonlinear heat fluxes to changes in TEM drive terms are shown. The response of these quantities to $1\sigma$ increases/decreases in $a/L_{T_e}$ (red), $a/L_n$ (blue), and $\nu_{ei}$ (green) around the ion heat flux-matched base case are plotted for the hollow discharge

The nonlinear gyrokinetic analysis of C-Mod plasmas presented here suggests that a clear transition from ITG to TEM does not accompany changes in particle transport and rotation profiles as previously reported on ASDEX-Upgrade [22]. We note that the relationship between changes in the the toroidal rotation and ITG to TEM transition has also been studied recently in Ohmic plasmas and auxiliary heated plasmas at Alcator C-Mod [47] and ASDEX-Upgrade [48, 18, 20]. In these works, no clear ITG to TEM transition appears responsible, but rather, more subtle changes in the turbulence correlate with the rotation and particle transport changes. The current work presented here is consistent with these findings [48, 18, 47, 20].

## 6. Discussion and Results

This paper presents analysis of two Alcator C-Mod L-mode discharges exhibiting significantly different profiles of toroidal rotation with approximately matched turbulence drive and suppression terms. The validation quality datasets obtained from these discharges and their extreme similarly makes them an ideal pair for testing recent theories related to impurity transport, rotation reversals, and transitions from core ITG to TEM dominated turbulence. Using updated profile analysis, new global, nonlinear gyrokinetic simulations were performed in both discharges that span the radial region r/a = 0.4 to 0.6. The updated analysis presented here improved agreement between the simulated and experimental impurity transport coefficients compared with previous work [29]. The impurity transport coefficients obtained from experiment were found to generally be in quantitative agreement with the updated simulation analysis (within

estimated uncertainties). Simulated peaking of impurities obtained from ion heat flux-matched simulation indicated peaked profiles in the range r/a = 0.4 to 0.6 for both the peaked and hollow rotation discharges. We note that, although analysis of these discharges results in a relatively small scan in Mach number, they exhibit significantly different values of the rotation gradient (u'). Unlike the database reported by Casson et al. [16], the C-Mod discharges do not exhibit a clear indication of dependence on rotation gradient. However, we note that this could be a result of our slightly smaller range in the rotation gradient or the smaller range in Mach numbers spanned by the peaked and hollow discharge relative to the ASDEX-Upgrade dataset.

Local, nonlinear gyrokinetic simulation was used to probe the response of the simulated ion heat flux to changes in the ITG drive term and to search for differences in the location of the ITG critical gradient and ion stiffness between the peaked and hollow discharges. A correlation between increased toroidal rotation and decreased ion stiffness was reported previously by Mantica *et al.* [11]. The work presented here attempted to leverage the significant difference in the toroidal rotation profiles from the peaked and hollow discharges and the similarity of most other simulation inputs, to explore any link between rotation and stiffness on Alcator C-Mod. The simulation results suggest that, despite the difference in the rotation profiles, the nonlinear ITG critical gradient and stiffness of the peaked and hollow discharges is indistinguishable and both plasma appear to display marginal stability to the ITG. These results appear inconsistent with work by Hahm and Yoon [2, 3], where it is suggested that an inward directed equipartiion momentum pinch plays a dominant role in plasmas exhibiting marginal stability to ITG.

Ion heat flux-matched simulations were obtained for both the hollow and peaked discharges, demonstrating the commonly observed $Q_e$ under-prediction [32]. To search for evidence of ITG to TEM discharges in these discharges, sensitivity scans in known TEM drive terms were performed around the ion heat flux-matched base case simulations. A slight dependency of the simulated heat fluxes on electron-ion collisionality was found in both discharges but can be explained by a decrease in the Dimits shift and a reduction of the ITG critical gradient reported by Mikkelsen *et al.* [46]. The sensitivity of the simulated heat fluxes to changes in TEM drive terms are all found to be negligibly small compared to the sensitivity to $a/L_{T_i}$. It is found that both discharges exhibit characteristics primarily found in ITG dominated plasmas and there is no evidence of significant subdominant TEM activity or any ITG to TEM transition. Therefore this simulation study finds no clear link between ITG/TEM transition and the measured rotation reversal in these discharges.

## 7. Acknowledgements

The authors would like to thank all of the Alcator C-Mod technical staff and the physics operators for their exceptional operation and maintenance of the tokamak. Specifically Dr. Amanda Hubbard for maintaining the ECE temperature measurements, Chi Gao for monitoring the XICS system for theses shots, Dr. Matt Reinke for processing ion

temperatures and rotations, Dr. Steve Wukitch for ICRF operation, Dr. Steve Wolfe for EFIT, and John Walk for processing of the density profiles. We would like to thank Dr. Ron Waltz for the development of the GYRO code. Computer simulations using GYRO were carried out at the National Energy Research Scientific Computing Center, which is supported by the Office of Science of the U.S. Department of Energy under Contract No. DE-AC02-05CH11231 and the MIT PSFC parallel AMD Opteron/Infiniband cluster Loki. This work was also supported by DOE contract - DE-FC02-99ER54512-CMOD and in part by an appointment to the US DOE Fusion Energy Postdoctoral Research Program administered by ORISE.

[1] P.H. Diamond, Y. Kosuga, .D. Grcan, C.J. McDevitt, T.S. Hahm, N. Fedorczak, J.E. Rice, W.X. Wang, S. Ku, J.M. Kwon, G. Dif-Pradalier, J. Abiteboul, L. Wang, W.H. Ko, Y.J. Shi, K. Ida, W. Solomon, H. Jhang, S.S. Kim, S. Yi, S.H. Ko, Y. Sarazin, R. Singh, and C.S. Chang. An overview of intrinsic torque and momentum transport bifurcations in toroidal plasmas. *Nuclear Fusion*, 53(10):104019, 2013.

[2] T. S. Hahm, P. H. Diamond, O. D. Gurcan, and G. Rewoldt. Nonlinear gyrokinetic theory of toroidal momentum pinch. *Physics of Plasmas (1994-present)*, 14(7):–, 2007.

[3] E.S. Yoon and T.S. Hahm. Transport of parallel momentum by toroidal ion temperature gradient instability near marginality. *Nuclear Fusion*, 50(6):064006, 2010.

[4] A. G. Peeters, C. Angioni, and D. Strintzi. Toroidal momentum pinch velocity due to the coriolis drift effect on small scale instabilities in a toroidal plasma. *Phys. Rev. Lett.*, 98:265003, Jun 2007.

[5] A. G. Peeters, C. Angioni, and D. Strintzi. Comment on turbulent equipartition theory of toroidal momentum pinch [phys. plasmas15, 055902 (2008)]. *Physics of Plasmas (1994-present)*, 16(3):–, 2009.

[6] C. Angioni et al. Particle pinch and collisionality in gyrokinetic simulations of tokamak plasma turbulence. *Physics of Plasmas*, **16**, (2009).

[7] R. Guirlet, D. Villegas, T. Parisot, C. Bourdelle, X. Garbet, F. Imbeaux, D. Mazon, and D. Pacella. Anomalous transport of light and heavy impurities in Tore Supra ohmic, weakly sawtoothing plasmas. *Nuclear Fusion*, 49(5):055007, 2009.

[8] T. Flp and H. Nordman. Turbulent and neoclassical impurity transport in tokamak plasmas. *Physics of Plasmas (1994-present)*, 16(3):–, 2009.

[9] T Hein and C Angioni. Electromagnetic effects on trace impurity transport in tokamak plasmas. *Physics of Plasmas (1994-present)*, 17(1):012307, 2010.

[10] N.T. Howard, M. Greenwald, D.R. Mikkelsen, M.L. Reinke, A.E. White, D. Ernst, Y. Podpaly, and J. Candy. Quantitative comparison of experimental impurity transport with nonlinear gyrokinetic simulation in an alcator c-mod l-mode plasma. *Nuclear Fusion*, 52(6):063002, 2012.

[11] P. Mantica, D. Strintzi, T. Tala, C. Giroud, T. Johnson, H. Leggate, E. Lerche, T. Loarer, A. G. Peeters, A. Salmi, S. Sharapov, D. Van Eester, P. C. de Vries, L. Zabeo, and K.-D. Zastrow. Experimental study of the ion critical-gradient length and stiffness level and the impact of rotation in the jet tokamak. *Phys. Rev. Lett.*, 102:175002, Apr 2009.

[12] P. Mantica, C. Angioni, C. Challis, G. Colyer, L. Frassinetti, N. Hawkes, T. Johnson, M. Tsalas, P. C. deVries, J. Weiland, B. Baiocchi, M. N. A. Beurskens, A. C. A. Figueiredo, C. Giroud, J. Hobirk, E. Joffrin, E. Lerche, V. Naulin, A. G. Peeters, A. Salmi, C. Sozzi, D. Strintzi, G. Staebler, T. Tala, D. Van Eester, and T. Versloot. A key to improved ion core confinement in the jet tokamak: Ion stiffness mitigation due to combined plasma rotation and low magnetic shear. *Phys. Rev. Lett.*, 107:135004, Sep 2011.

[13] J. Citrin, F. Jenko, P. Mantica, D. Told, C. Bourdelle, J. Garcia, J. W. Haverkort, G. M. D.

Hogeweij, T. Johnson, and M. J. Pueschel. Nonlinear stabilization of tokamak microturbulence by fast ions. *Phys. Rev. Lett.*, 111:155001, Oct 2013.

[14] J. Citrin, F. Jenko, P. Mantica, D. Told, C. Bourdelle, R. Dumont, J. Garcia, J.W. Haverkort, G.M.D. Hogeweij, T. Johnson, M.J. Pueschel, and JET-EFDA contributors. Ion temperature profile stiffness: non-linear gyrokinetic simulations and comparison with experiment. *Nuclear Fusion*, 54(2):023008, 2014.

[15] P. H. Diamond, C. J. McDevitt, . D. Grcan, T. S. Hahm, and V. Naulin. Transport of parallel momentum by collisionless drift wave turbulence. *Physics of Plasmas (1994-present)*, 15(1):–, 2008.

[16] F.J. Casson, R.M. McDermott, C. Angioni, Y. Camenen, R. Dux, E. Fable, R. Fischer, B. Geiger, P. Manas, L. Menchero, G. Tardini, and the ASDEX Upgrade Team. Validation of gyrokinetic modelling of light impurity transport including rotation in asdex upgrade. *Nuclear Fusion*, 53(6):063026, 2013.

[17] A. G. Peeters, C. Angioni, and the ASDEX Upgrade Team. Linear gyrokinetic calculations of toroidal momentum transport in a tokamak due to the ion temperature gradient mode. *Physics of Plasmas (1994-present)*, 12(7):–, 2005.

[18] C. Angioni, R. M. McDermott, F. J. Casson, E. Fable, A. Bottino, R. Dux, R. Fischer, Y. Podoba, T. Pütterich, F. Ryter, and E. Viezzer. Intrinsic toroidal rotation, density peaking, and turbulence regimes in the core of tokamak plasmas. *Phys. Rev. Lett.*, 107:215003, Nov 2011.

[19] M. Barnes, F. I. Parra, J. P. Lee, E. A. Belli, M. F. F. Nave, and A. E. White. Intrinsic rotation driven by non-maxwellian equilibria in tokamak plasmas. *Phys. Rev. Lett.*, 111:055005, Aug 2013.

[20] C. Angioni, Y. Camenen, F.J. Casson, E. Fable, R.M. McDermott, A.G. Peeters, and J.E. Rice. Off-diagonal particle and toroidal momentum transport: a survey of experimental, theoretical and modelling aspects. *Nuclear Fusion*, 52(11):114003, 2012.

[21] J.E. Rice, B.P. Duval, M.L. Reinke, Y.A. Podpaly, A. Bortolon, R.M. Churchill, I. Cziegler, P.H. Diamond, A. Dominguez, P.C. Ennever, C.L. Fiore, R.S. Granetz, M.J. Greenwald, A.E. Hubbard, J.W. Hughes, J.H. Irby, Y. Ma, E.S. Marmar, R.M. McDermott, M. Porkolab, N. Tsujii, and S.M. Wolfe. Observations of core toroidal rotation reversals in alcator c-mod ohmic l-mode plasmas. *Nuclear Fusion*, 51(8):083005, 2011.

[22] R M McDermott, C Angioni, R Dux, E Fable, T Ptterich, F Ryter, A Salmi, T Tala, G Tardini, E Viezzer, and the ASDEX Upgrade Team. Core momentum and particle transport studies in the asdex upgrade tokamak. *Plasma Physics and Controlled Fusion*, 53(12):124013, 2011.

[23] B P Duval, A Bortolon, A Karpushov, R A Pitts, A Pochelon, A Scarabosio, and the TCV Team. Bulk plasma rotation in the tcv tokamak in the absence of external momentum input. *Plasma Physics and Controlled Fusion*, 49(12B):B195, 2007.

[24] J. E. Rice, I. Cziegler, P. H. Diamond, B. P. Duval, Y. A. Podpaly, M. L. Reinke, P. C. Ennever, M. J. Greenwald, J. W. Hughes, Y. Ma, E. S. Marmar, M. Porkolab, N. Tsujii, and S. M. Wolfe. Rotation reversal bifurcation and energy confinement saturation in tokamak ohmic l-mode plasmas. *Phys. Rev. Lett.*, 107:265001, Dec 2011.

[25] H Nordman, A Skyman, P Strand, C Giroud, F Jenko, F Merz, V Naulin, T Tala, and the JET-EFDA Contributors. Fluid and gyrokinetic simulations of impurity transport at jet. *Plasma Physics and Controlled Fusion*, 53(10):105005, 2011.

[26] R M McDermott, C Angioni, R Dux, A Gude, T Ptterich, F Ryter, G Tardini, and the ASDEX Upgrade Team. Effect of electron cyclotron resonance heating (ecrh) on toroidal rotation in asdex upgrade h-mode discharges. *Plasma Physics and Controlled Fusion*, 53(3):035007, 2011.

[27] J. Candy and R. E. Waltz. Anomalous transport scaling in the DIII-D tokamak matched by supercomputer simulation. *Phys. Rev. Lett.*, 91:045001, Jul 2003.

[28] M L Reinke, J E Rice, A E White, M Greenwald, N T Howard, P Ennever, C Gao, A E Hubbard, and J W Hughes. Density sensitivity of intrinsic rotation profiles in ion cyclotron range of frequency-heated l-mode plasmas. *Plasma Physics and Controlled Fusion*, 55(1):012001, 2013.

[29] A. E. White, N. T. Howard, M. Greenwald, M. L. Reinke, C. Sung, S. Baek, M. Barnes, J. Candy, A. Dominguez, D. Ernst, C. Gao, A. E. Hubbard, J. W. Hughes, Y. Lin, D. Mikkelsen, F. Parra, M. Porkolab, J. E. Rice, J. Walk, S. J. Wukitch, and Alcator C-Mod Team. Multi-channel transport experiments at alcator c-mod and comparison with gyrokinetic simulations. *Physics of Plasmas*, 20(5):056106, 2013.

[30] A. Ince-Cushman, J. E. Rice, M. Bitter, M. L. Reinke, K. W. Hill, M. F. Gu, E. Eikenberry, Ch. Broennimann, S. Scott, Y. Podpaly, S. G. Lee, and E. S. Marmar. Spatially resolved high resolution x-ray spectroscopy for magnetically confined fusion plasmas (invited). *Review of Scientific Instruments.*, 79(10):10E302, 2008.

[31] M L Reinke, I H Hutchinson, J E Rice, N T Howard, A Bader, S Wukitch, Y Lin, D C Pace, A Hubbard, J W Hughes, and Y Podpaly. Poloidal variation of high- Z impurity density due to hydrogen minority ion cyclotron resonance heating on Alcator C-Mod. *Plasma Physics and Controlled Fusion*, 54(4):045004, 2012.

[32] N.T. Howard, A.E. White, M. Greenwald, M.L. Reinke, C. Holland, J. Candy, and J.R. Walk. Validation of the gyrokinetic model in itg and tem dominated l-mode plasmas. *Nuclear Fusion*, 53(12):123011, 2013.

[33] http://w3.pppl.gov/transp/.

[34] R. E. Waltz and R. L. Miller. Ion temperature gradient turbulence simulations and plasma flux surface shape. *Physics of Plasmas*, 6(11):4265–4271, 1999.

[35] J. Candy and R. E. Waltz. Velocity-space resolution, entropy production, and upwind dissipation in eulerian gyrokinetic simulations. *Physics of Plasmas (1994-present)*, 13(3):–, 2006.

[36] J. Candy and E. Belli. *GYRO Reference Guide*. General Atomics, 2013.

[37] N. T. Howard, A. E. White, M. Greenwald, M. L. Reinke, J. Walk, C. Holland, J. Candy, and T. Gorler. Investigation of the transport shortfall in alcator c-mod l-mode plasmas. *Physics of Plasmas*, 20(3):032510, 2013.

[38] J Candy, R E Waltz, M R Fahey, and C Holland. The effect of ion-scale dynamics on electron-temperature-gradient turbulence. *Plasma Physics and Controlled Fusion*, 49(8):1209, 2007.

[39] R. E. Waltz, J. Candy, and M. Fahey. Coupled ion temperature gradient and trapped electron mode to electron temperature gradient mode gyrokinetic simulations. *Physics of Plasmas*, 14(5):056116, 2007.

[40] T. Görler and F. Jenko. Scale separation between electron and ion thermal transport. *Phys. Rev. Lett.*, 100:185002, May 2008.

[41] E A Belli and J Candy. Kinetic calculation of neoclassical transport including self-consistent electron and impurity dynamics. *Plasma Physics and Controlled Fusion*, 50(9):095010, 2008.

[42] F. Jenko, W. Dorland, M. Kotschenreuther, and B. N. Rogers. Electron temperature gradient driven turbulence. *Physics of Plasmas*, 7(5):1904–1910, 2000.

[43] A. Bortolon, B. P. Duval, A. Pochelon, and A. Scarabosio. Observation of spontaneous toroidal rotation inversion in ohmically heated tokamak plasmas. *Phys. Rev. Lett.*, 97:235003, Dec 2006.

[44] F Wagner and U Stroth. Transport in toroidal devices-the experimentalist's view. *Plasma Physics and Controlled Fusion*, 35(10):1321, 1993.

[45] C. L. Rettig, T. L. Rhodes, J. N. Leboeuf, W. A. Peebles, E. J. Doyle, G. M. Staebler, K. H. Burrell, and R. A. Moyer. Search for the ion temperature gradient mode in a tokamak plasma and comparison with theoretical predictions. *Physics of Plasmas (1994-present)*, 8(5):2232–2237, 2001.

[46] D. R. Mikkelsen and W. Dorland. Dimits shift in realistic gyrokinetic plasma-turbulence simulations. *Phys. Rev. Lett.*, 101:135003, Sep 2008.

[47] C. Sung, A.E. White, N.T. Howard, C.Y. Oi, J.E. Rice, C. Gao, P. Ennever, M. Porkolab, F. Parra, D. Mikkelsen, D. Ernst, J. Walk, J.W. Hughes, J. Irby, C. Kasten, A.E. Hubbard, M.J. Greenwald, and the Alcator C-Mod Team. Changes in core electron temperature fluctuations across the ohmic energy confinement transition in alcator c-mod plasmas. *Nuclear Fusion*, 53(8):083010, 2013.

[48] R.M. McDermott, C. Angioni, G.D. Conway, R. Dux, E. Fable, R. Fischer, T. Ptterich, F. Ryter, E. Viezzer, and the ASDEX Upgrade Team. Core intrinsic rotation behaviour in asdex upgrade ohmic l-mode plasmas. *Nuclear Fusion*, 54(4):043009, 2014.